High-power test and thermal characteristics of a new radio-frequency quadrupole cavity for the Japan Proton Accelerator Research Complex linac

Yasuhiro Kondo,* Takatoshi Morishita, Kazuo Hasegawa, Etsuji Chishiro, Koichiro Hirano,
Toshihiko Hori, Hidetomo Oguri, Fumiaki Sato, and Shinichi Shinozaki

Japan Atomic Energy Agency (JAEA), Tokai, Naka, Ibaraki, 319-1195, Japan

Takashi Sugimura, Hiroshi Kawamata, Fujio Naito, Yuji Fukui, Kenta Futatsukawa, and Kesao Nanmo

High Energy Accelerator Research Organization (KEK), Tsukuba, Ibaraki, 305-0801, Japan

We performed a high-power test of a new radio-frequency quadrupole (RFQ II) for the J-PARC linac. RFQ II was developed as a spare RFQ because the operating J-PARC RFQ has suffered from a sparking problem. First, the conditioning of RFQ II was carried out; after 50 h of conditioning, RFQ II became very stable with a nominal power and duty of 330 kW and 3%, respectively. Next the thermal properties were measured because the resonant frequency of RFQ II is tuned by changing the temperature of the cooling water. The frequency response was measured and compared to finite-element method simulation results, confirming that the simple two-dimensional model reproduces the experimental data well. The differences in the field distribution with changes in the rf loading and the cooling-water temperature were also measured, and no serious field distortion was observed. Therefore, we conclude that RFQ II can perform well as a high-power rf cavity.

PACS numbers: 29.20.Ej

I. INTRODUCTION

The Japan Proton Accelerator Research Complex (J-PARC) is a multipurpose facility for particle physics, nuclear physics, materials and life science, and so on. The J-PARC accelerator consists of a 400-MeV linac, a 3-GeV rapid-cycling synchrotron [1], and a 50-GeV main ring [2]. The original design energy and peak beam current of the linac are 400 MeV and 50 mA, respectively, although, in the initial phase, operation began with an energy of 181 MeV, omitting the annular-ring coupling structures [3]. A four-vane-type radio-frequency quadrupole (RFQ) built for the Japan hadron facility project is used for the initial phase linac; the design peak beam current of this RFQ is 30 mA [4]. Because a sparking problem occurred in this RFQ [5], another RFQ was newly fabricated [6] as a spare for the operating RFQ. We call this spare RFQ II, whereas the operating one is called RFQ I [7]. Table I lists the design parameters of RFQ II.

The beam dynamics design of RFQ II is the same as that of RFQ I; however, in designing the RFQ II cavity, various points that would cause discharge problems in RFQ I were greatly improved as follows.

(i) The rf structure of RFQ I is installed in a large vacuum vessel. The surface area of this type of system is very large; thus, it is difficult to obtain good vacuum quality. Therefore, a vacuum-tight cavity structure is adopted for RFQ II. To this end, we adopted brazing for the assembly method [6]. In the final stage of brazing, the temperature of the cavity surface reaches more than 800°C. At this temperature, the damaged layer by machining is recrystallized, decreasing the defects that make the electronic structure of the surface unstable. Additionally, attached substances are baked out during the brazing process; thus, the finished surface is very clean. These features also contribute to improving the resistance to discharging.

TABLE I. Design parameters of J-PARC RFQ II.

Beam species	H^-
Resonant frequency	324 MHz
Injection energy	50 keV
Extraction energy	3 MeV
Peak beam current	30 mA
Vane length	3172 mm
Average bore radius (r_0)	3.69 mm
ρ_t/r_0 ratio[a]	0.89 (ρ_t = 3.28 mm)
Intervane voltage	82.9 kV
Maximum surface field	31.6 MV/m (1.77 Kilpatrick)
Nominal peak power	330 kW
Repetition rate	50 Hz[b]
rf pulse length	600 μs
Duty	3%

[a]ρ_t: transverse radius of the vane tip.
[b]The requirement for RFQ II is 25 Hz but RFQ II is designed to withstand 50 Hz.

*yasuhiro.kondo@j-parc.jp

YASUHIRO KONDO *et al.*

Phys. Rev. ST Accel. Beams **16,** 040102 (2013)

(ii) The material of the RFQ I cavity is 0.2% silver-doped oxygen-free copper (OFC) because it is easier to machine. In contrast, for RFQ II, pure OFC was used to prioritize resistance to discharging over machinability. Moreover, RFQ I tends to start discharging after a certain operating time; therefore, hot isostatic pressing (HIP) [9] is applied to the material of the RFQ II cavity to prevent the vane tip from absorbing gases during operation.

(iii) Specially ordered concave-formed cutters were used to machine the vane tips of RFQ I; however, the machining friction of the formed cutters is rather large, so the surface machined with them tends to be rough. Therefore, commercially available ball-nose cutters were used for machining of the RFQ II vane tips [10]. In addition, to remove the fine edges formed by ball-nose cutters, chemical polishing [11] was adopted.

(iv) RFQ I was equipped with π-mode stabilizing loops (PISLs) [12] to prevent dipole mode mixing. However, we decided not to use the PISLs and adopted a four-rod-type dipole stabilizer (DSR) [13] for RFQ II [14], because the PISLs are suspected of being a potential source of discharging and multipacting. The electric-field strength between the PISL and its penetration is almost the same as that of the intervane field, and the complicated structure of the PISL would be a source of gas emission and multipacting.

(v) The final point is that the mechanical autotuners were discarded to improve the mechanical reliability. Instead, the resonant frequency is fine-tuned during the operation by adjusting the temperature of the cooling water, as in other RFQs [15,16].

In this paper, the high-power test results for J-PARC RFQ II, which is improved compared to RFQ I as noted above, are described. In particular, related to the last point listed above, we performed experiments on frequency tuning by cooling-water-temperature control, and the results are presented. First, in Sec. II, the details of the experimental apparatus are presented, and in Sec. III, the conditioning results are shown. Then, the model used to simulate the thermal properties is described in Sec. IV, and the results of experiments on the thermal characteristics and a comparison to the simulations results are discussed in Sec. V. Finally, in Sec. VI, we summarize the paper.

II. EXPERIMENTAL APPARATUS

Figures 1 and 2 show a schematic drawing and a cross-sectional view of J-PARC RFQ II, respectively. In Fig. 2, the upper right quadrant is denoted as Q1, the upper left is Q2, the lower left is Q3, and the lower right is Q4; right and left are defined as viewed from upstream.

RFQ II consists of three longitudinally segmented unit cavities, and the vane lengths of the units are 1057.2, 1053.6, and 1061.3 mm, respectively. One unit cavity consists of upper and lower major vanes and left and right
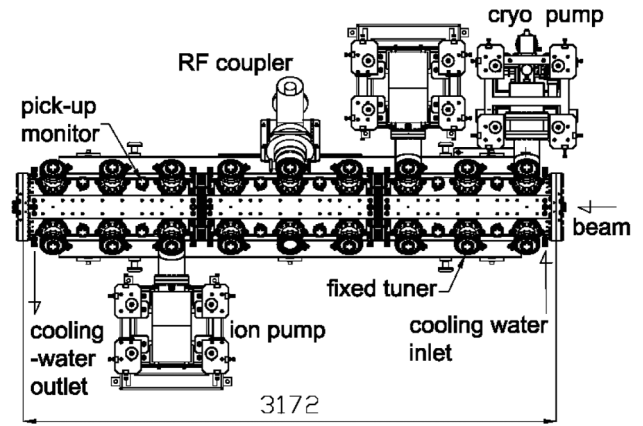
FIG. 1. Schematic of RFQ II (top view).
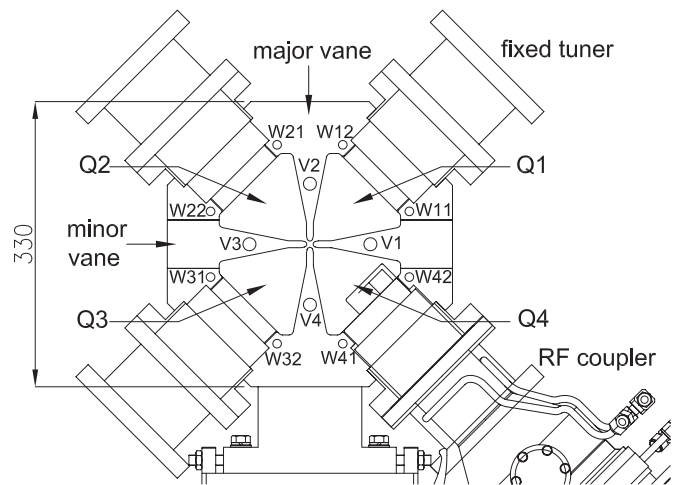
FIG. 2. Cross-sectional view (viewed from upstream) of RFQ II.

minor vanes. The major and minor vanes were joined by vacuum brazing. The material of the cavity is OFC class 1 [17], and HIP treatment was applied to reduce the voids between the crystal grains, as mentioned in Sec. I.

The resonant-frequency error and field distortion due to fabrication error are corrected using fixed tuners. The fixed slug tuner is slitted and also works as a vacuum port. Q4 has eight fixed tuners, and the other quadrants have nine fixed tuners each; thus, the total number of fixed tuners is 35.

Vacuum pumping is possible from all ports except the radio-frequency (rf) coupler port, but in the present experiments, a 1700 L/s (for N_2) cryopump was attached to the first port (from upstream) of Q4, and two 400 L/s ion pumps were attached to the eighth port of Q3 and the third port of Q4, respectively. The pressure was measured with a Bayard-Alpert (BA) gauge attached to the most downstream port of Q4.

In the center port of Q4, a loop-type rf coupler was inserted. The rf power was generated by a 324-MHz klystron (Toshiba E3740A [18]). The rf power was transmitted

via WR2300 rectangular waveguides to the vicinity of RFQ II, transformed to WX203D coaxial waveguides, reduced to 152D, and finally reduced to 77D by the rf coupler.

The field distribution during operation can be measured with loop-type pickup monitors. Six pickups are installed in each quadrant; thus, the total number of pickups is 24.

To adjust the resonant frequency by controlling the cooling-water temperature, RFQ II is equipped with two types of cooling-water channels. Four channels are used to cool the vanes, and the other eight channels are used to cool the cavity walls. In Fig. 2, V1, V2, ... are vane cooling channels, and W11, W12, ... are wall cooling channels. The resonant frequency of an RFQ cavity f is represented as $f = \frac{1}{2\pi\sqrt{LC}}$, where L is the inductance of a current circulating among the cavity wall and vanes, and C is the capacitance between the vane tips. By denoting the cross-sectional area of a quadrant as A and the intervane gap length as d, the relations $L \propto A$ and $C \propto d^{-1}$ can be derived. Therefore, by adjusting the wall-water temperature T_w and vane-water temperature T_v, L and C can be controlled individually. Methods of adjusting either T_v and T_w while keeping the other temperature constant are available, but at this time, T_v was adjusted because the frequency response is faster than that obtained by changing T_w. The diameter of the vane channels is 15 mm and that of the wall channels is 10 mm. The water flows in each channel are parallel from the low-energy end to the high-energy end, and the channels of three unit cavities are serially connected. The water channels of the three fixed tuners are connected serially, and the end plates and rf coupler each have a water channel. The water temperatures at the exits of all the channels are measured with resistance

thermometers (PT100), and the flow rates are measured with float-type flow meters.

To verify the frequency tuning using the cooling-water temperature, a compact water-temperature-control unit for the RFQ high-power test was developed. The water from this unit is used for the vane channel, and the water supplied from the utility of the J-PARC linac at a constant temperature is used for the wall channel. Figures 3 and 4 show a schematic diagram and a photograph of this unit, respectively.

The 27°C water from the utility is cooled using a 25-kW heat exchanger. The flow rate into this unit is measured with a flow indicator, FI1. The temperature at the exit of the heat exchanger (temperature of supply water to the vane channel T_{vs}) is measured with a temperature-indicating controller, TIC1. This temperature is compared with a target temperature, and heat removal is controlled by driving a three-way motor-operated valve, MV6, at the

FIG. 4. Photograph of the water-temperature-control unit.
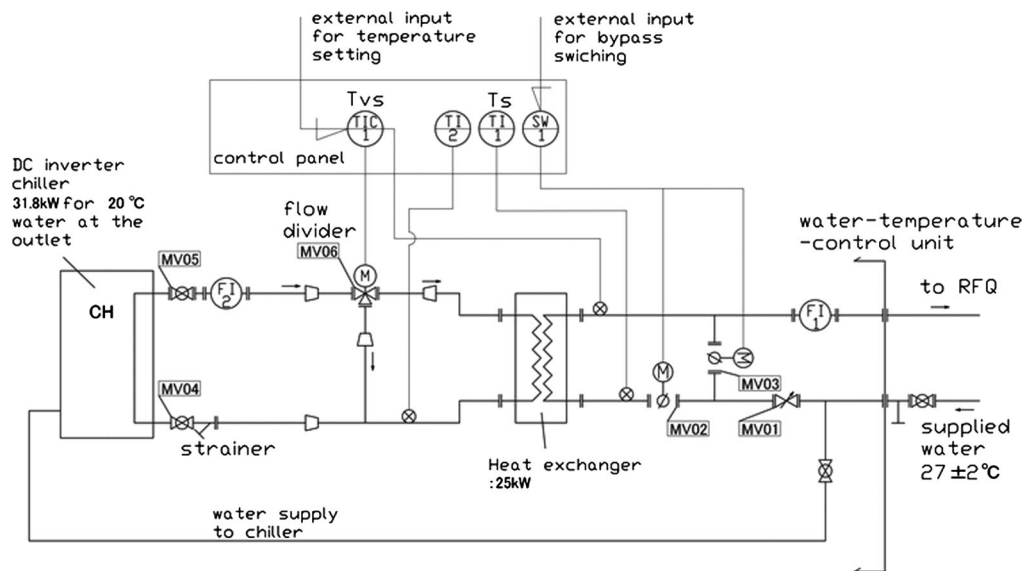
FIG. 3. Schematic of the water-temperature-control unit for RFQ high-power test.
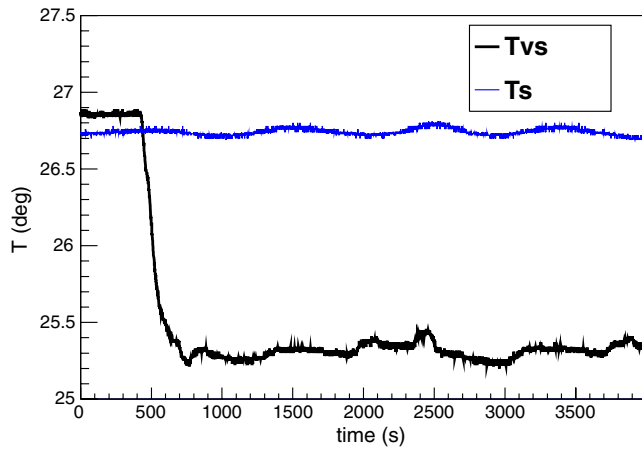
FIG. 5. Stability of water-temperature-control unit. Tvs is the temperature of the water provided to the vane channel, and Ts is that of the water supplied to this unit. At $t = 430$ s, Tvs was changed from 26.9 to 25.3°C, and after about 300 s, Tvs became stable within ± 0.13°C.

cooler-side (primary) water passage using a proportional-integral-derivative control method. The temperature of the water supplied by the utility, Ts, is measured and indicated by TI2. All the temperature sensors are PT100. The maximum suppliable flow rate of this unit is 100 L/ min , but for the high-power test of RFQ II, this unit was used with a flow rate of 80 L/ min ; at this flow rate, the variable range of Tvs was 24–27°C. The target temperature of Tvs can be set via the front panel of the unit and also by an external voltage input to the TIC1. The primary water is cooled by a DC inverter unit chiller (Daikin UWAXP8BPA5 [19]), and the temperature and flow rate are measured by FI2 and TI2, respectively. Additionally, the unit has valves, MV2 and MV3, to bypass this unit. These valves can also be remote controlled, providing an external signal to switch SW1.

Figure 5 shows the stability of this unit. In this figure, the target temperature of Tvs was changed to 25.3°C at $t = 430$ s. After about 300 s, Tvs became stable within ± 0.13°C.

III. CONDITIONING RESULTS

In this section, the conditioning results for RFQ II are described. RFQ II was conditioned at a 324-MHz high-power test stand in the J-PARC linac building. Figure 6 is a photograph of RFQ II under high-power conditioning.

After all the components were assembled, the measured unloaded Q value was 9436. This corresponds to 87% of a SUPERFISH [20] calculation. The coupling factor of the rf coupler was set to 1.7. The vacuum pressure inside the cavity was measured with a BA gauge, and the rf power was turned off if the pressure exceeded 1.0×10^{-4} Pa.

Figure 7 shows the conditioning history of RFQ II. First, the pulse width and repetition rate were set to 30 μs and 25 Hz, respectively. After 15 h of conditioning, the peak

FIG. 6. Photograph of RFQ II under conditioning. This photograph shows the view from upstream, and the rf power is fed from the right side of the picture.
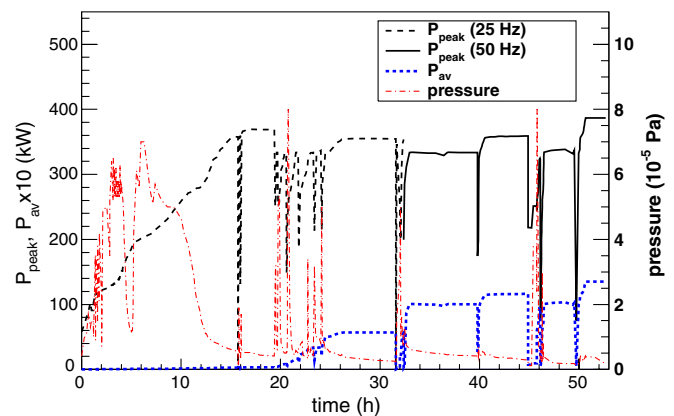
FIG. 7. Conditioning history of RFQ II.

power P_{peak} reached 360 kW; this is 10% higher than the nominal peak power of 330 kW. The pulse width was gradually broadened to 600 μs, and then the repetition rate was increased to 50 Hz. Finally, the conditioning was continued until P_{peak} reached 390 kW with a pulse width of 600 μs and a repetition rate of 50 Hz. In Fig. 7, the dashed and solid (black) lines represent P_{peak} at repetition rates of 25 and 50 Hz, respectively. The dotted line (blue) is the averaged power P_{av}, and the dash-dotted (red) line represents the vacuum pressure in the cavity. After conditioning up to 390 kW, a 24-h operation test was conducted at the nominal power. During the 24-h operation, trips occurred only 3 times, and it was confirmed that RFQ II can be operated stably.

IV. MODELING

In designing RFQ II, two-dimensional finite-element method (FEM) analyses were performed [21] to estimate the frequency tuning range by changing the water temperature. It is easy to make a model for a two-dimensional simulation, and calculation is fast; however, it is a simple model that omits detailed cavity structures such as the fixed

tuners and end part of the cavity. Therefore, it is essential to verify the model by comparing it with experimental data. In this section, the simulation method is reviewed briefly, and the parameter tuning of the model for comparison with the experimental results is described.

The temperature distribution and deformation due to heat loading of the RFQ were analyzed using ABAQUS [22]. First, the distribution of the heat load on the cavity surface was calculated using SUPERFISH, and this was input to ABAQUS. Subsequently, the steady-state temperature distribution in the cavity cross section was derived, as shown in Fig. 8. Using this distribution, the deformations of each segment, dx and dy, from the initial state, which is a uniform 27°C, were calculated with ABAQUS. Finally, using the above dx and dy, the frequency shift Δf was calculated from the df/dx and df/dy values of each segment obtained with SUPERFISH.

The heat convection factor h and power dissipation to the model were tuned to reproduce the measured values of the temperature rises ΔT listed in Table II; they were measured at $P_{\text{peak}} = 330$ kW and a duty of 3%. Tv1, Tv2, ... are the water temperatures at the exits of the vane channels V1, V2, …, and Tw11, Tw12, ... are those of the wall channels W11, W12, and so on. Moreover, Tv$_{av}$ and Tw$_{av}$ are the averaged temperatures at the exits of the vane and wall channels, respectively. At that time, the flow rates were 20 L/min for the vane channels and 12 L/min for the wall channels. Taking account of the temperature rises through the cooling-water channels, the averaged water temperature between the rf-on and -off states were used for the cooling-water temperatures in the simulation Tv$_{\text{sim}}$ and Tw$_{\text{sim}}$; that is, both Tv$_{\text{sim}}$ and Tw$_{\text{sim}}$ were 27.2°C. The derivation scheme for Tv$_{\text{sim}}$ and Tw$_{\text{sim}}$ is described in the next section. The temperature rises of each cooling water per unit length
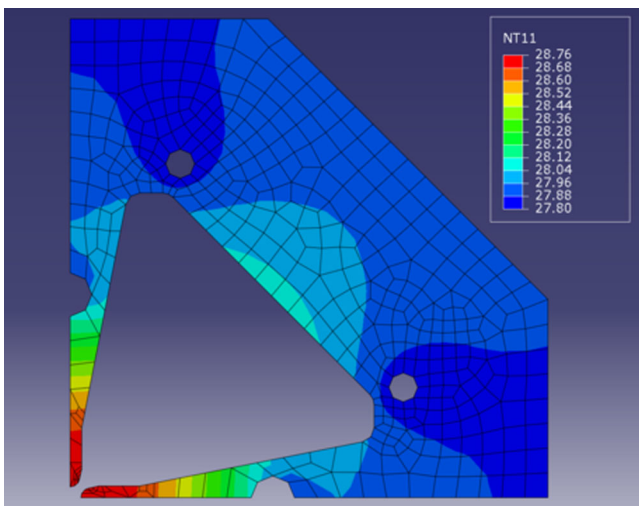
TABLE II. Measured temperature rise of each cooling-water channel with $P_{\text{peak}} = 330$ kW and a duty of 3%. rf-off and rf-on indicate the temperatures at the exit of each channel when rf power is fed and not fed, respectively. ΔT denotes the difference between rf-on and rf-off.

	rf-off (°C)	rf-on (°C)	ΔT (°C)
Tv1	26.87	27.50	0.64
Tv2	26.96	27.58	0.63
Tv3	26.86	27.48	0.62
Tv4	26.93	27.51	0.58
Tv$_{av}$	26.90	27.52	0.62
Tw11	26.90	27.49	0.59
Tw12	26.88	27.51	0.62
Tw21	26.87	27.49	0.63
Tw22	26.85	27.46	0.61
Tw31	26.99	27.57	0.58
Tw32	26.88	27.47	0.60
Tw41	26.87	27.45	0.58
Tw42	26.86	27.46	0.61
Tw$_{av}$	26.89	27.49	0.60

can be derived from the power dissipation to each channel, which depends on h. The h values were tuned to reproduce the measured values ΔTv$_{av}$ and ΔTw$_{av}$ normalized by the vane length. The obtained h values are 7800 W/m²K for the vane channel and 8200 W/m²K for the wall channels. In this case, the calculated frequency shift from the rf-off state is 34 kHz, and the experimental result was 30 kHz.

V. EXPERIMENTAL RESULTS

In this section, the experimental results for verifying the model calculation described in the previous section are presented.

Figure 9 shows the frequency shifts from the rf-off state as a function of vane-water temperature. The closed circles represent the measured data, and the open squares are the simulation results. The horizontal axis represents the vane-water temperature. For the experimental data, the vane-water temperature is the averaged value of Tvs and Tv$_{av}$, and this value was used for the simulation as Tv$_{\text{sim}}$. The supplied water temperature for the cavity wall Tws was not varied; however, the temperature rises of the wall channels also change if Tvs is varied because the heat dissipation to the wall channel depends on the vane-water temperature. Therefore, the averaged value between the measured values Tws and Tw$_{av}$ was used as the wall-water temperature for the simulation, Tw$_{\text{sim}}$. The frequency responses to the change in the vane-water temperature obtained by linear fitting are 34 kHz/°C for the experiment and 32 kHz/°C for the simulation. The slope of the frequency shift to the vane-water temperature is reproduced well.

Next, the transient behavior when the status is changed from rf-on to rf-off is indicated in Fig. 10. The closed circles are the measured values, and the open squares are

FIG. 8. Temperature distribution calculated with ABAQUS. The water temperatures of both the vane and wall channels are 27.2°C. NT11 denotes the temperature at each node.
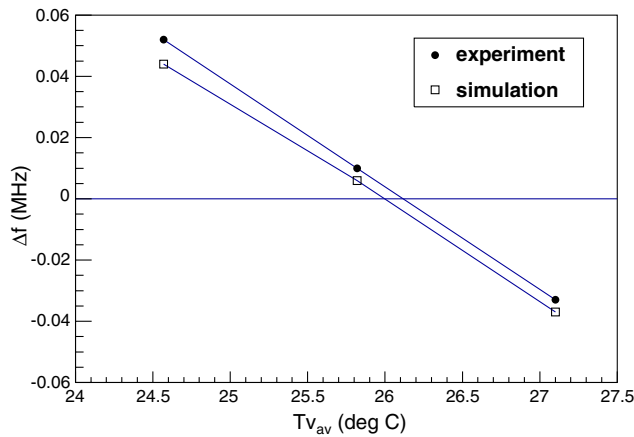
FIG. 9. Frequency response as a function of temperature of vane water. The vertical axis indicates the frequency shift from the rf-off state.
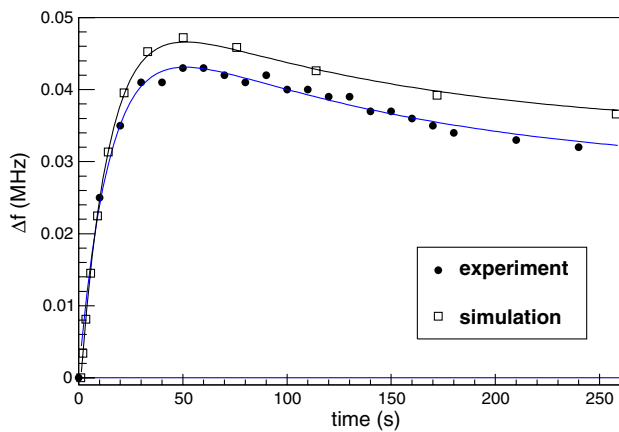
FIG. 10. Transient behavior after the rf power is turned off. The rf power was turned off at $t = 0$. The vertical axis is the frequency shift from $t = 0$.

the simulation. The horizontal axis represents the time after rf is turned off. The vertical axis denotes the frequency shift from $t = 0$. At that time, Tv_{av} was 26.29°C and Tw_{av} was 27.06°C. Both the measured and simulation data are fitted with

$$\Delta f = c_1 + c_2 \exp\left(\frac{t}{\tau_1}\right) + c_3 \exp\left(\frac{t}{\tau_2}\right). \quad (1)$$

In Fig. 10, the solid lines are the fitting results, and the fitting parameters are listed in Table III. The time constants of the measurement and simulation agreed with each other within 8%.

Finally, the uniformity of the electromagnetic field was confirmed. If the resonant frequency is tuned by changing the vane water, the heat dissipation to the vane water becomes larger with decreasing temperature; thus, the temperature difference between the inlet and outlet of the water channel becomes larger. With the present setup, Tvs can be decreased to 24°C, and the temperature rise through

TABLE III. Fitting results for the transient experiment and simulation.

	c_1 (MHz)	c_2 (MHz)	τ_1 (s)	c_3 (MHz)	τ_2 (s)
Experiment	0.028	-0.052	-15	0.024	140
Simulation	0.034	-0.059	-14	0.020	-130

the entire vane length is 1.2°C. This temperature rise corresponds to 40 kHz according to the measured frequency response mentioned above. Supposing that the frequency shift is linear from the inlets to the outlets, the field distortion of the fundamental TE210 mode due to this frequency shift is estimated to be about 0.1%, which is negligibly small, by the perturbation method [23]. However, due to imperfections in the machining and fabrication, the distortion may be larger than expected. Thus, we investigated the field difference from no rf loading to the rf-on state, and also to the state with decreased vane-water temperature.

Figure 11 shows the change ratios of the field measured by pickup monitors. The upper figure represents the ratio of the variation in the voltage $\Delta V/V$ from a pulse width of 30 μs and repetition rate of 50 Hz (duty 0.15%) to those of 600 μs and 50 Hz, keeping both Tvs and Tws at 27°C. The initial duty state, 0.15%, simulates the no-rf-loading state. The field uniformity measured with the bead-pull method
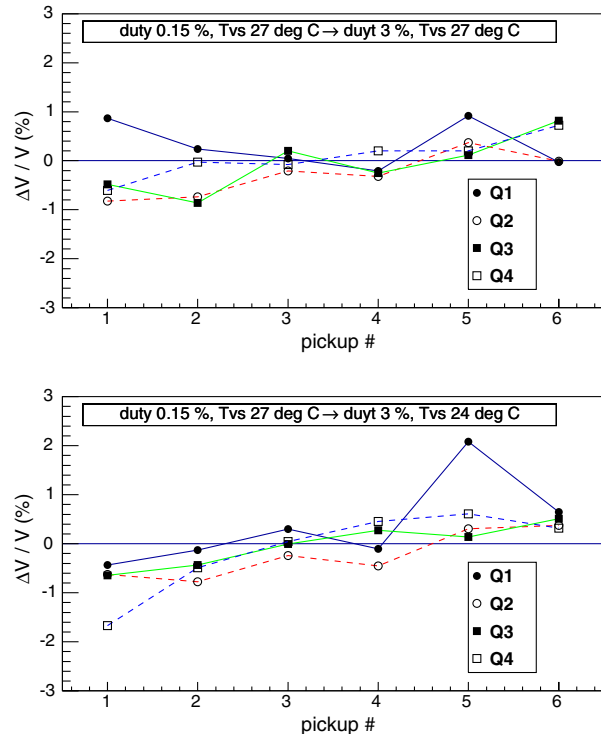
FIG. 11. Field distributions measured by pickup monitors. The upper figure represents the voltage difference $\Delta V/V$ between a duty factor of 0.15% and 3% keeping Tvs = 27°C. The lower figure is $\Delta V/V$ from Tvs = 27°C and duty = 0.15% to Tvs = 24°C and duty = 3%.

TABLE IV.   PARMTEQM simulation results for field tilt. Here, ε_t is the normalized rms transverse emittance, and ε_l is the longitudinal emittance.

Tilt (%)	Transmission (%)	ε_t (π mm mrad)	ε_l (π MeV deg)
0	97.7	0.18	0.84
2	97.5	0.18	0.84

was within $\pm 1.5\%$. In the lower figure, $\Delta V/V$ of T vs $=$ 24°C from the initial low duty state is shown. From this figure, the field appears slightly tilted from the initial state. Therefore, estimating on the highest side, the effect of a 2% tilt on the beam dynamics was simulated using PARMTEQM [24]; a 2% tilt means that the voltage on the entrance end is 2% below the average voltage and that on the exit end is 2% above the average. In this simulation, the peak current of the input beam was 36 mA, the normalized rms transverse emittance was 0.17π mm mrad, the transverse distribution was a water-bag distribution, the input energy was 50 keV, and the phase distribution was uniform.

Table IV lists the simulation results. From this result, a 2% tilt has very little effect on the quality of the beam; thus, the measured field change from no rf loading is not a problem.

VI. CONCLUSION

A high-power test of J-PARC RFQ II was successfully conducted. In designing and fabricating RFQ II, various improvements from the first J-PARC RFQ (RFQ I) were made to increase the resistance to discharging. After 50 h of conditioning, the peak power reached 390 kW, which corresponds to 118% of the nominal power of 330 kW, with a pulse width of 600 μs and a repetition rate of 50 Hz. Moreover, 24-h operation with the nominal peak power was very stable. The resonant-frequency response to the vane-water temperature was investigated and compared to a two-dimensional FEM model. The measured frequency response was 34 kHz/°C, and the simulated response was 32 kHz/°C. The transient behavior was also measured, and the time constants of the measurement and simulation agreed with each other within 8%. These results confirm that this simple FEM model is valid for using the RFQ design to predict the frequency response. Additionally, the electromagnetic field distributions at low duty (0.15%), nominal duty (3%), and different vane-water temperature (27°C and 24°C) were measured. The field differences from the low duty state were within 2%; this has a very small effect on beam dynamics. The results above fully confirmed the soundness of J-PARC RFQ II as a high-power rf cavity.

ACKNOWLEDGMENTS

[1] H. Hotchi, in *Proceedings of IPAC2011, San Sebastián, Spain* (EPS-AG, Spain, 2011), pp. 6–10.

[2] T. Koseki, in Proceedings of IPAC2011, San Sebastián, Spain (Ref. [1]), pp. 2499–2501.

[3] K. Hasegawa, in *Proceedings of the 2007 Particle Accelerator Conference, Albuquerque, New Mexico* (IEEE, New York, 2007), pp. 2619–2623.

[4] A. Ueno and Y. Kondo, in *Proceedings of the 20th International Linac Conference, Monterey, CA, 2000* (SLAC, Menlo Park, CA, 2000), pp. 545–547.

[5] K. Hasegawa, T. Kobayashi, Y. Kondo, T. Morishita, H. Oguri, Y. Hori, C. Kubota, H. Matsumoto, F. Naito, and M. Yoshioka, in *Proceedings of IPAC2010* (ICR, Kyoto, Japan, 2010), pp. 621–623.

[6] T. Morishita, Y. Kondo, K. Hasegawa, F. Naito, M. Yoshioka, H. Matsumoto, Y. Hori, H. Kawamata, Y. Saito, and H. Baba, in *Proceedings of LINAC2010* (KEK, Tsukuba, Japan, 2010), pp. 521–523.

[7] After the fabrication of RFQ II, the development of another RFQ with a design current of 50 mA was begun. This RFQ is called RFQ III [8], and its purpose is to upgrade the beam current of the J-PARC linac to achieve the original design power of 1 MW (at the neutron target).

[8] Y. Kondo, K. Hasegawa, T. Morishita, and R. A. Jameson, Phys. Rev. ST Accel. Beams **15**, 080101 (2012).

[9] H. Matsumoto, M. Akemoto, H. Hayano, A. Miura, T. Naito, and S. Takeda, in *Proceedings of PAC91* (APS Beam Physics, San Francisco, California, 1991), pp. 1008–1010.

[10] T. Morishita *et al.*, in Proceedings of LINAC2010 (Ref. [6]), pp. 518–520.

[11] T. Morishita, Y. Kondo, H. Kazuo, K. Hiroshi, S. Takashi, and N. Fujio, in Proceedings of LINAC2012 (Tel-Aviv, Israel, 2012).

[12] A. Ueno and Y. Yamazaki, Nucl. Instrum. Methods Phys. Res., Sect. A **300**, 15 (1991).

[13] L. M. Young, in *Proceedings of LINAC1994* (KEK, Tsukuba, Japan, 1994), pp. 178–180.

[14] The separation between the TE210 and the nearest dipole modes was estimated to be adjusted from 3 to 5 MHz with DSRs in simulation. However, in actual measurement, the separation was optimum, that is 5 MHz, when the DSRs were 0 mm. Therefore, actual RFQ II is not equipped with DSRs.

[15] R. Floersch and G. Domer, in *Proceedings of the 19th International Linear Accelerators Conference, Chicago, Illinois, 1998* (NTIS, Springfield, VA, 1998), pp. 992–994.

[16] S. Virostek and J. Staples, in Proceedings of the 20th International Linac Conference, Monterey, CA, 2000 (Ref. [4]), pp. 908–910.

[17] Hitach Cable Ltd. [http://www.hitachi-cable.com].

[18] Toshiba Electron Tubes and Devices Co. Ltd. [http://www.toshiba-tetd.co.jp/eng/].

[19] Daikin Industries Ltd. [http://www.daikin.com].

[20] J. H. Billen and L. M. Young, Technical Report No. LA-UR-96-1834, 1996.

[21] Y. Kondo *et al.*, in Proceedings of IPAC2010 (Ref. [5]), pp. 780–782.

[22] Dassault Systèmes, "ABAQUS" [http://www.3ds.com/products/simulia/portfolio/abaqus/].

[23] T. P. Wangler, *RF Linear Accelerators* (Wiley-VCH, Weinheim, 2008), 2nd ed.

[24] K. R. Crandall, T. P. Wangler, L. M. Young, J. H. Billen, G. H. Neuschaefer, and D. L. Schrage, Los Alamos National Laboratory Technical Report No. LA-UR-96-1836, 1996.